Chemical Physics Letters 678 (2017) 65–71

Contents lists available at ScienceDirect

Chemical Physics Letters

journal homepage: www.elsevier.com/locate/cplett

Research paper

Broadband terahertz dielectric spectroscopy of alcohols

Sohini Sarkar, Debasis Saha, Sneha Banerjee, Arnab Mukherjee *, Pankaj Mandal *

Department of Chemistry, Indian Institute of Science Education and Research (IISER), Pune 411008, India

ARTICLE INFO

Article history:
Received 27 February 2017
In final form 8 April 2017
Available online 9 April 2017

Keywords:
Time-domain terahertz spectroscopy
Alcohols
Dielectric functions
Intermolecular vibrations

ABSTRACT

We have studied the complex dielectric properties of a series of alcohols in 0.5–10 THz frequency range using THz time-domain spectroscopy. The dielectric response observed has contribution from a Debye relaxation process and three damped harmonic oscillators. Combination of experimental observations, all-atom molecular dynamics simulations and *ab initio* quantum calculations reveals that the complex dielectric spectra of alcohols result from a complex dynamics involving vibrational motions of several atoms across multiple interacting alcohol molecules. The major contribution comes from the fast hydrogen-bond rupture and reformation dynamics, the motion of alkyl chains, and the motions of the H-bonded OH groups.

1. Introduction

Hydrogen bond (H-bond) dynamics plays a pivotal role in various chemical and biological phenomena. Water, the solvent of life, is probably the most studied H-bonded liquid [1]. Alcohols are another important class of H-bonded liquids, but are not studied extensively. Unlike water, alcohol molecules can donate only one hydrogen bond but can accept two [2] lacking the extensive H-bond network that is present in water. Secondly, the amphiphilic alcohol molecules have both polar hydroxyl hydrophilic part, capable of forming H-bond, and non-polar alkyl hydrophobic part engendering hydrophobic interaction between molecules in the condensed phase. A change in the size and shape of the hydrophobic part can alter the hydrophobic interactions and may also affect the H-bond network. Moreover, alcohols are miscible with myriads of polar and non polar solvents. Studies on the molecular structure of liquid alcohols using X ray scattering, MD simulations, etc. reveal that alcohol molecules associate to form ring or chain like structure [3]. However, the degree of association is still debatable. Also, the relation between the structure and dynamics is not yet well understood. NMR relaxation experiments suggest that with increasing alkyl chain length the rotational correlation time of the OH group slows down from methanol (~5 ps) to 1-hexanol (~90 ps) [4]. Using OH stretching mode as an indicator, polarization sensitive pump probe and 2D IR spectroscopy have recently been employed to understand H-bond dynamics in alcohols [5]. The study reveals that OH dynamics predominantly has two timescales; a fast component (~100 fs) assigned to librations and H-Bond stretching, common for both water and alcohols, and a slower component (a few picoseconds) arising from the diffusion-dictated H-Bond exchange dynamics present only in alcohols. In another recent study, Hunger et al. used polarization resolved fs-IR spectroscopy to show that the OD stretch vibration is faster for methanol (~0.75 ps) compared to ethanol (~0.9 ps) and its higher homologues [6].

Dielectric spectroscopy provides further insights into the reorientation dynamics of the alcohols [7]. This method records the response of polar molecules to an applied oscillating electric field in the form of dielectric loss and dispersion functions which result from the reorientation of molecular dipoles. Thus, the frequency dependent complex permittivity, $\epsilon(\nu) = \epsilon'(\nu) - i\epsilon''(\nu)$, can be measured. This, in turn, provides the relaxation time (τ_j) and dispersion amplitudes ($\Delta\epsilon_j$) of the fundamental relaxation processes. Alcohols show three distinct relaxation dynamics in the timescales of one to hundreds of picoseconds depending on the size of the alcohol molecule: (a) a slow relaxation process originating from the alignment of dipoles in the H-bonded network, (b) an intermediate relaxation process stemming from the reorientation of alcohol monomers, and (c) a very fast process related to the flipping or rotation of the free OH group or breaking and reformation of H-Bond in a translational motion [8].

At terahertz (THz) (1 THz = 33.33 cm^{-1} = 4 meV) frequency range (0.1–15 THz), the molecular reorientation and several intermolecular vibrations (local oscillations of dipoles) may coexist contributing to the overall liquid dynamics. Nevertheless, dielectric properties in THz frequency regime remained unexplored for a long time since this region of the electromagnetic spectrum could not be accessed until recently [9]. Time domain THz spectroscopy

* Corresponding authors.
E-mail addresses: arnab.mukherjee@iiserpune.ac.in (A. Mukherjee), pankaj@iiserpune.ac.in (P. Mandal).

http://dx.doi.org/10.1016/j.cplett.2017.04.026
0009-2614/

(THz TDS) technique measures the electric field, rather than intensity, and thus provides both the amplitude and phase of the spectral components making up the THz pulse. From the amplitude and phase, absorption coefficient and refractive index of the sample can be calculated. This allows for the evaluation of the complex-valued permittivity of the sample without involving Kramers-Kronig analysis [9b].

Kindt and Schmuttenmaer initiated the study of dielectric properties of methanol, ethanol, 1-propanol utilizing THz-TDS in the narrow frequency range of 0.06–1.0 THz [10]. They found a good agreement between their data and multiple relaxation models up to 1 THz. At higher frequencies, there is an onset of oscillatory motions, which cannot be fitted using relaxation models. Kindt et al., however, did not observe the onset of resonant absorption till 1 THz, necessitating the measurement of dielectric properties at higher frequencies. Fukasawa et al. analyzed the complex dielectric and Raman spectra of H-bond liquids from microwave to THz frequency range combining microwave and far infrared (FIR) techniques [11]. Their study reveals that the dielectric spectrum for methanol deviates from the relaxation model at frequencies above $\nu \sim$ 290 GHz. Three Debye relaxation processes (τ_1 = 51.8 ps, τ_2 = 8.04 ps, and τ_3 = 0.89 ps) combined with two damped oscillators with peaks at ~55 and 125 cm^{-1} reproduced the dielectric spectrum of methanol within 50 MHz–5 THz frequency range [11]. Yomogida et al. studied temperature dependent complex permittivity of 14 monohydric alcohols in the frequency range of 0.2–2.5 THz. According to their study, the complex permittivity of the alcohols has contribution from three parts: the high frequency part of the dielectric relaxation, a broad vibrational mode around 1.2 THz, and a low frequency tail of another high frequency oscillatory motion located above 2.5 THz [12]. However, the precise nature of this high frequency mode and its effect to the dynamics could not be ascertained since the study was limited to 2.5 THz.

In the present study, broadband THz-TDS (0.5–10 THz) has been utilized to study the dielectric properties of methanol, ethanol, 1-propanol, 2-propanol, and 1-butanol. We have also performed all-atom molecular dynamics (MD) simulations and *ab initio* quantum calculations of the alcohols to gain the molecular level understanding of the vibrational modes responsible for the observed absorption pattern in the THz region.

2. Methods and Materials

2.1. Terahertz time domain spectroscopy (THz-TDS)

In our laboratory, we generate pulsed THz waves from ambient air plasma and detect them using air-biased coherent detection (ABCD) technique [13]. ABCD enables detection of broadband THz generated from air plasma since it is not limited by phonon absorption, dispersion, or damage threshold that otherwise restrict the THz bandwidth detection by other methods such as electro-optic sampling and photo current measurement on a photoconductive switch [13]. The entire THz setup is purged with dry nitrogen to remove water vapor, an aggressive absorber of THz light. Relative humidity of <2% has been maintained during the experiments. The details regarding our THz setup (Fig. S1) are described in the Supporting Information (SI). The spectral bandwidth detected in our lab is often more than 15 THz (see Fig. S2). However, in the present study we have restricted all spectral analyses to the frequency range of 0.5–10 THz because the amplitude of THz field drops below 1/e of the maximum amplitude at frequencies below 0.5 THz. Also, there is considerable absorption by the alcohols above 10 THz, making the transmission very poor. The sample cell comprising two high resistivity silicon windows (2 mm thickness, 1 in. diameter) separated by polytetrafluoroethylene (PTFE) spacer was placed at the focal point of two parabolic mirrors. First, the THz field transmitted through an empty cell was recorded as the reference signal ($E_{cell}(t)$). Next, THz signal transmitted through the sample cell filled with alcohol was measured ($E_{sam}(t)$). To obtain a satisfactory signal-to-noise (S/N) ratio, an average of several measurements (normally 30–50) was carried out. The shape, amplitude, and the phase of $E_{sam}(t)$ differ from $E_{cell}(t)$ due to the reflection, absorption, and dispersion of THz light by the sample. Exact Blackman windowing function was applied to the time domain signal prior to the Fourier transformation. By taking the ratio of complex Fourier transformation of $E_{sam}(t)$ and $E_{cell}(t)$, the complex refractive index of the sample can be obtained as,

$$\frac{fE_{sam}(t)}{fE_{cell}(t)} = \frac{\tilde{E}_{sam}(\omega)}{\tilde{E}_{cell}(\omega)} = \sqrt{T(\omega)}\exp(i\varphi(\omega)), \quad (1)$$

where $T(\omega)$ is the power transmittance and $\varphi(\omega)$ is the relative phase. The Fresnel reflection and transmission losses were considered while extracting the complex refractive index ($\tilde{n}(\omega) = n_{re}(\omega) + in_{im}(\omega)$) from $T(\omega)$ and $\varphi(\omega)$ using an iterative method following Nashima et al. [14]. An average spectrum for each alcohol was obtained from measurements using three different path lengths (100, 150, and 250 μm) at the room temperature.

2.2. Materials

The alcohols studied in this work are methanol, ethanol, 1-propanol, 2-propanol, and 1-butanol. Methanol and 1–butanol (purity 99.8%) were purchased from Sigma Aldrich. Ethanol (purity ≥ 99.9%) was purchased from Merck. 1-Propanol and 2-propanol (HPLC grade, 99.8% purity) were procured from Rankem. All alcohol samples were used without further purification.

2.3. Computational study

We used both classical and quantum approaches to understand the interactions amongst alcohol molecules within the THz frequency range in molecular detail. Classical molecular dynamics simulations were used to generate vibrational density of states (VDOSs) and normal modes. We also performed quantum calculations to compare the modes at different frequencies obtained from classical simulations and also to calculate H-bond strengths of alcohols. Details of the method are provided below.

2.3.1. Molecular dynamics (MD) simulation. MD simulations were performed using OPLS (Optimized Potential for Liquid Simulations) force field for all systems (methanol, ethanol, 1-propanol, 2-propanol and 1-butanol) [15]. For each system, a cubic box was created and was filled with alcohol molecules for simulation. The simulations were carried out by employing periodic boundary condition in all directions to mimic the effect of the bulk. The number of molecules taken in the simulations were: 631 for methanol, 501 for ethanol, 501 for 1-propanol, 465 for 2-propanol and 424 for 1-butanol. Each system was energy minimized using steepest descent method [16], followed by heating up to 300 K using Berendsen thermostat [17] with a coupling constant of 0.2 ps. This was followed by an equilibration run for 5 ns at constant temperature (300 K) and 1 bar pressure using Nosé-Hoover thermostat [18] and Parrinello-Rahman barostat [19], respectively, with a coupling constant of 0.2 ps for each. Particle Mesh Ewald (PME) method [20] with 10 Å cut-off was used for electrostatic interactions. Experimental compressibility [21] was used to achieve the correct density. A cut-off of 10 Å was used for the van der Waals interactions. All the simulations were carried out using GROMACS [22] software package.

2.3.2. Vibrational density of states (VDOS) calculation. We have calculated VDOS from both the velocity autocorrelation function (VACF) and normal mode analyses (NMA). In the first approach,

VDOS was calculated from the Fourier transformation of the velocity autocorrelation function (VACF) of all the atoms of the system defined as,

$$I(\omega) = \frac{1}{k_B T}\sum_j m_j\left[\frac{1}{2\pi}\int_{-\infty}^{\infty}\exp(-i\omega t)\boldsymbol{v}_j(0).\boldsymbol{v}_j(t)dt\right],$$

where $\boldsymbol{v}_j(t)$ is the velocity of the jth atom at time t. To calculate the VACF, the equilibrated structure was simulated for 1 ns under the same conditions as the equilibration run and the frames were saved at every 5 fs. An initial 500 ps long trajectory was sufficient to get a smooth VACF profile. For the calculation of VDOS using normal mode analysis, 10 frames were extracted from the 1 ns trajectory at 100 ps intervals and the Hessian matrix was generated for every frame. Diagonalization of the Hessian matrix provided the normal modes (vibrational spectrum) of different frequencies. The final vibrational spectrum was obtained from the average of 10 different vibrational spectra for each alcohol system. Both the VACF calculation and the normal mode analyses were carried out using GROMACS [22] software package. The modes at the frequency range obtained from fitting of the experimental data were plotted using Gaussview software [23].

2.3.3. Ab-initio Calculations. Random configurations consisting of four or five alcohol molecules were collected from MD simulations and were optimized using density functional theory (DFT) with B3LYP functional [24] and 6-31G(d,p) basis set. We used B3LYP functional because it shows a good agreement with experimental frequencies for several systems reported by Czarnecki et al. [25]. However, we used here a smaller basis set to reduce computational cost. Frequency calculations were performed on the optimized configurations to obtain the vibrational spectrum. Twenty configurations were used to obtain an average spectrum for each system. Similar approach has been used before for ion-water systems [26]. Moreover, we calculated H-bonding strength of different alcohols by calculating the quantum mechanical energy as a function of H-bond distance between the oxygen and hydrogen atoms of a H-bonding pair using Second-order Møller–Plesset (MP2) method with aug-cc-pVDZ [27] basis set. All quantum calculations were performed using Gaussian09 software package [28].

3. Results and discussion

3.1. THz-TDS

The time domain and Fourier transformed frequency domain data of the empty sample cell, and that filled with methanol and 1-butanol are shown in Fig. 1a and 1b, respectively. The time domain and Fourier transformed frequency domain data of other alcohols are shown in Figs. S3 and S4 in SI, respectively. From the frequency domain data, we have extracted the frequency dependent absorptions and refractive indices (Fig. 2a and b). The errors associated with the refractive index values of the alcohols studied are given in Table S1. In all cases, the error is between 2–6%.

The absorption spectrum of methanol (Fig. 2a) shows a prominent absorption peak at ~3.8 THz (~127 cm^{-1}) and a broad peak at ~8 THz (~266 cm^{-1}). These two absorption features are clearly visible in case of ethanol as well. However, for all other alcohols studied here the absorption feature at about 4–5 THz is visible, and seems to have shifted towards a higher frequency with the increasing number of carbon atoms in the alcohol molecule. Note that, methanol has a strikingly higher absorbance compared to other alcohols almost throughout the entire frequency range.

The absorbance decreases in alcohols with increasing alkyl chain length. It is interesting to note that the absorption spectra of 1-propanol and 2-propanol are quite different even though the numbers of carbon atoms are same in both molecules. This probably indicates that 2-propanol having a branched hydrophobic part exhibits different structure and dynamics than its isomer 1-propanol.

However, the absorption and refractive index data can only provide the information on the optical properties of the medium. A better insight into the liquid dynamics can be obtained from the frequency dependent complex dielectric function as defined below.

$$\hat{\epsilon}(\omega) = \epsilon'(\omega) - i\epsilon''(\omega). \quad (2)$$

The complex dielectric constant and the complex refractive index are related as,

$$\hat{n}(\nu) = n(\nu) - ik(\nu), \quad (3)$$

$$\epsilon'(\omega) = n^2(\omega) - k^2(\omega), \quad (4)$$

$$\epsilon''(\omega) = 2n(\omega)k(\omega), \quad (5)$$

where $\omega = 2\pi\nu$ and $k(\omega) = \frac{\lambda\alpha(\omega)}{4\pi} = \frac{c\alpha(\omega)}{2\omega}$. α is the absorption coefficient, λ is the wavelength, and c is the speed of light in vacuum. Fig. S5a and S5b in SI respectively show the frequency dependent real and imaginary components of the dielectric functions of different alcohols. The error in evaluating the real and imaginary dielectric function values using three spacer sizes is 4–10% and 6–15%, respectively. Details are provided in Tables S2 and S3 of SI. The errors in our measurements are mainly due to the uncertainty in the sample path length, and are similar to that reported by Kindt et al. [10]. The real and imaginary values of dielectric function obtained here are in good agreement (within error bars) with the previous literature reports in the common frequency range (0.5–2.5 THz) [11,12].

An inflection point at ~4 THz is observed in the dielectric dispersion of methanol (Fig. S5a). Corresponding to this there is a peak in the dielectric loss spectrum (Fig. S5b). To understand various relaxation processes contributing to the dielectric spectra of the alcohols, we tried fitting the dielectric dispersion and dielectric loss spectra using a Debye relaxation model. According to this model, the complex permittivity is given by,

$$\hat{\epsilon}(\omega) = \epsilon_\infty + \sum_{j=1}^{n}\frac{\epsilon_j - \epsilon_{j+1}}{1 + i\omega\tau_j}, \quad (6)$$

where ω is the angular frequency, ϵ_1 is the static dielectric constant, ϵ_j's are the strengths of dielectric relaxation processes, ϵ_∞ is the dielectric constant at high frequency, n is the number of relaxation processes, and τ_j's are the relaxation times. However, the Debye relaxation model, even with the inclusion of multiple relaxation times, failed to provide an acceptable fit (determined by χ^2 and correlation coefficient value) to the experimental data.

As mentioned above, lower frequency limit of our experimental data in this study is 0.5 THz which is much higher than the frequency for which Debye relaxation models were used in earlier reports [8b,c]. Furthermore, Fukasawa et al. reported that at frequencies ~290 GHz, there is a significant discrepancy between the experimental dielectric spectrum of methanol and its fit to the Debye model [11]. Therefore, only Debye relaxation may not be an appropriate model to describe the dielectric function of alcohols beyond 0.5 THz. At higher THz frequencies, resonant or oscillatory motions of a molecule or a group of molecules come into play [10]. Such motions are apparent in the absorptions that are associated with inflection points in the refractive index graph. In such cases, Debye relaxation model may become inadequate; instead damped harmonic oscillator model has to be used to understand the oscillatory motions of the molecules. Accordingly, we attempted fitting the dielectric spectra using different models

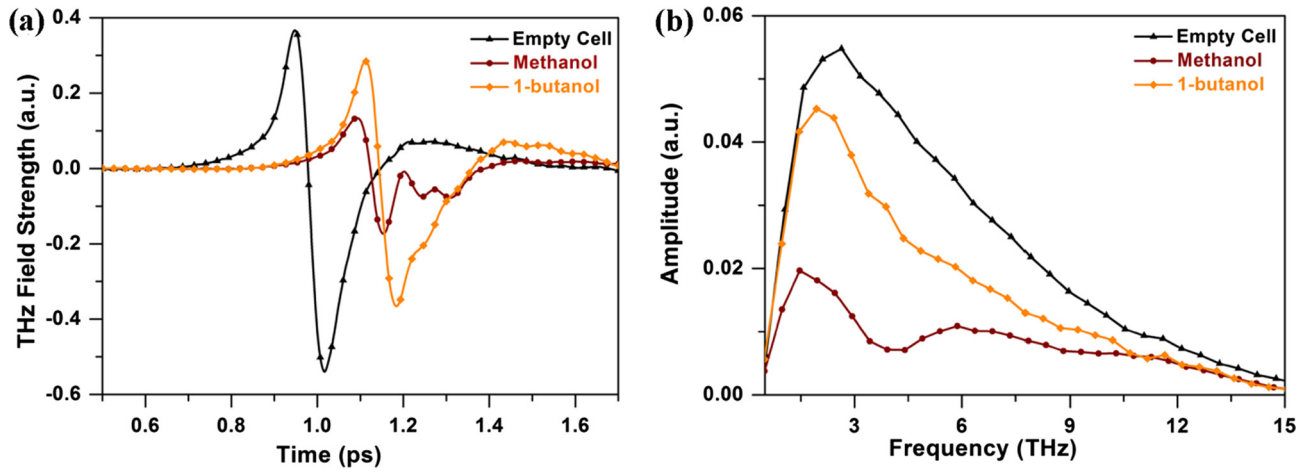

Fig. 1. (a) Time domain THz waveforms and corresponding, (b) frequency domain amplitude spectra of empty sample cell and cells filled with methanol and 1-butanol (path length 150 μm).

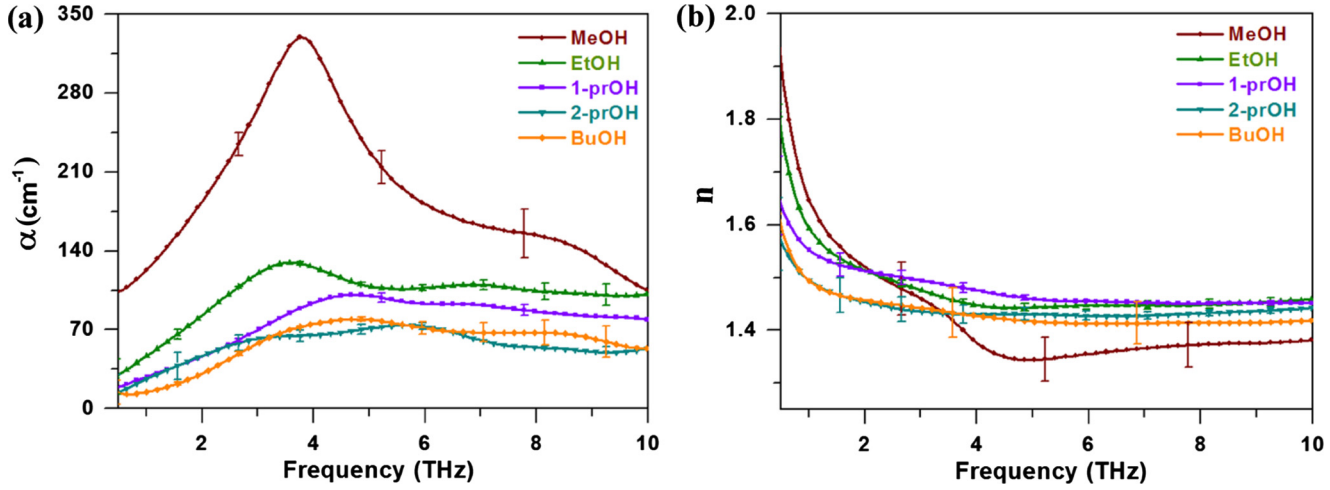

Fig. 2. Frequency dependent (a) absorption and (b) real refractive indices of alcohols. Error bars for some selected frequency only are shown to preserve clarity. Note that, the errors are large at the extremes of the frequency range.

that are combinations of Debye relaxation and damped harmonic oscillator models. The complex dielectric spectrum in oscillator model is given by,

$$\hat{\epsilon}(\omega) = \sum_{i=1}^{n} \frac{A_i}{\omega_i^2 - \omega^2 - i\omega\gamma_i}, \tag{7}$$

where A_i is the amplitude of the oscillatory motion, ω_i is the angular frequency, and γ_i is the damping coefficient. Among all combinations attempted, only the model with single Debye and three oscillators could simultaneously fit the experimentally observed real and imaginary dielectric functions. The χ^2 values of the fits were less than 0.001 and correlation coefficient values were very close to 1 (Table S4 in SI), ensuring good fit to the experimental data. Fig. 3 shows the experimental real and imaginary dielectric functions of the alcohols and their fits to single Debye and triple oscillator model. The complex equation combining single Debye and three damped harmonic oscillator model is given by,

$$\hat{\epsilon}(\omega) = \epsilon_\infty + \frac{\Delta\epsilon}{1 + i\omega\tau} + \frac{A_1}{\omega_1^2 - \omega^2 - i\omega\gamma_1} + \frac{A_2}{\omega_2^2 - \omega^2 - i\omega\gamma_2} + \frac{A_3}{\omega_3^2 - \omega^2 - i\omega\gamma_3}. \tag{8}$$

Table 1 lists the relaxation time and oscillator frequencies obtained on fitting the experimental dielectric functions to Eq. (8). There is a relaxation process occurring at the time scale of 0.7–2 ps for all alcohols studied. The timescales we obtain by fitting the dielectric function of alcohols are also very similar to the timescale of rupture and reformation of individual H-bonds in alcohols and water reported earlier [29]. Hence, we assign the Debye relaxation process contributing to our broadband THz data to the H-bond breaking and reforming dynamics.

We obtain three peaks from fitting the experimental dielectrics for all the alcohols studied here. The first peak is at a low frequency of 1–2 THz. A major peak for all the alcohols is found in 4–6 THz range. The third peak is obtained at a frequency above 8 THz. The frequency range of our study is limited to 10 THz. Therefore, the reliability associated with the high frequency peaks obtained from the fits is expected to be less. Fig. S6 in SI shows the contributions of the Debye relaxation and the three oscillators to the experimentally observed dielectric loss spectrum for methanol. To understand the origin of these peaks, we have used computational methods to identify the modes corresponding to different frequencies.

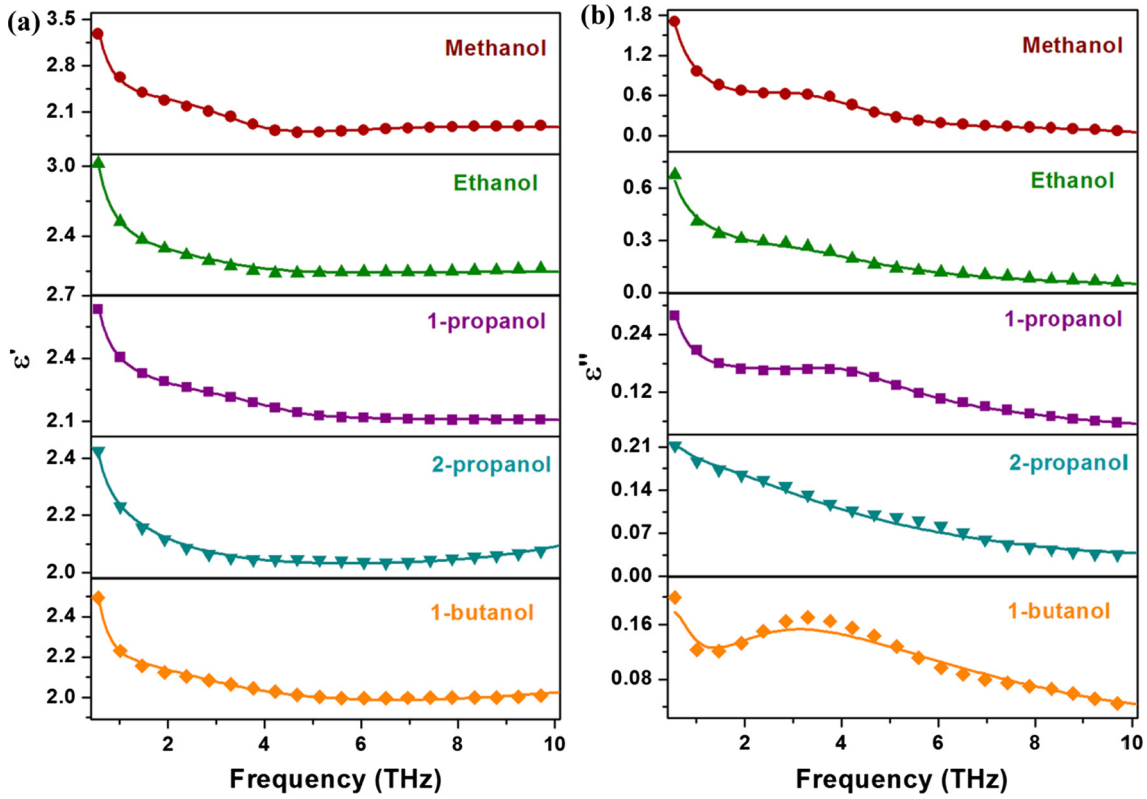

Fig. 3. Experimental dielectric functions (symbols) of the alcohols and their fits (solid lines) to Debye-oscillator combined model (Eq. (8)). The left and right panels portray the real (ε′) and imaginary (ε′) components of the dielectric functions, respectively.

Table 1
Debye and oscillator model parameters from fitting of the experimental data to the combined single Debye and triple damped harmonic oscillator model. The other parameters of the fits are given in Table S4 in SI.

Alcohols	τ (ps)	ω_1 (THz)	ω_2 (THz)	ω_3 (THz)
Methanol	0.78 ± 0.03	0.94 ± 0.07	3.68 ± 0.05	7.9 ± 0.2
Ethanol	0.82 ± 0.03	1.9 ± 0.7	3.82 ± 0.09	9.54 ± 2.1
1-Propanol	1.10 ± 0.01	1.87 ± 0.05	4.38 ± 0.02	9.5 ± 1.1
2-Propanol	2.01 ± 0.22	1.9 ± 0.2	5.09 ± 0.14	13.5 ± 0.5
1-Butanol	1.12 ± 0.06	2.4 ± 0.9	4.9 ± 0.35	15.6 ± 2.2

3.2. Vibrational spectra from classical simulation

Classical simulations enable us to obtain the vibrational spectra for the entire system at a finite temperature using velocity autocorrelation function (VACF). The vibrational spectra calculated using VACF is shown in Fig. 4. To compare with experimental results, only the relevant frequency range (1–10 THz) of the spectra is shown. This region of the spectrum primarily involves intermolecular interactions among different molecules.

As observed from the experimental values, here also we find a peak below 2 THz frequency region. However, the broad peak observed at the low frequency region is known to correspond to intermolecular collision modes, as seen for other systems [30]. Similar to experiment, methanol shows a peak close to 4 THz not seen for other alcohols for which several different peaks are observed in the region above 6 THz. The spectral feature within 2–6 THz region is similar. Note that, however, the VDOS calculated using VACF as shown above involves all Raman and IR active modes whereas the experimental data presented here have contribution only from IR active modes.

To visualize the atomistic motions at a given frequency, we performed normal mode analyses (NMA) of the system collected at

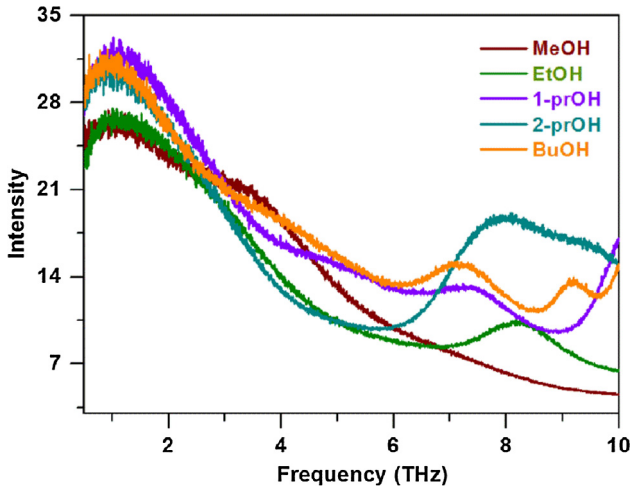

Fig. 4. A specific THz region of the spectra of different alcohols generated using VACF.

100 ps interval from the simulation and plotted in Fig. S7 in SI. Vibrational spectra from NMA are similar for all the alcohols. Although the spectral features are similar, it does not show any peak for methanol at 4 THz or at higher frequency for other alcohols. The difference between both approaches may be the reason for this discrepancy. While VACF has dynamical information at a finite temperature and therefore represent the quasi-harmonic modes, NMA represents the result based on a given local minimum with harmonic approximation.

NMA reveals that the modes at around 2 THz for different alcohols correspond to the collective motions of the whole molecule as shown in Fig. S8 in SI. Woods et al. also observed an absorption band around 30 cm^{-1} (0.9 THz) in their FIR spectroscopic study of liquid methanol [31]. However, they assigned the 30 cm^{-1} band to the intermolecular bending. The other major peak in the experiment was found at around 4–6 THz region. Modes at this frequency range correspond to the vibration of the alkyl groups with smaller movements of OH groups. These motions for methanol, ethanol and 1-propanol are shown in Fig. 5, whereas those for 2-propanol and 1-butanol are given in Fig. S9 in SI. Note here that, in our analysis we find the movements of the H-atoms more predominant compared to the motions of the heavier atoms. However from the magnitude of these movements, as shown by the different sized arrows in Fig. 5, we determine the motions of the atoms responsible for peaks at different frequency ranges.

3.3. Frequencies from ab initio method

Since NMA suffers from the inaccuracies of classical force-field, we performed *ab initio* calculations to verify and compare different vibrational modes at the frequencies observed in experiment. However, quantum calculations are extremely computationally expensive. Therefore, only a subset of system representing the first solvation shell of a particular alcohol molecule was considered for the calculation. To capture the effect of temperature and various configurational arrangements of molecules, we collected around 20 snapshots at around 100 ps interval. In case of methanol, five molecules were selected. For the other alcohols, only four were selected to reduce computational cost. Also, we did not consider the configurations where there was no hydrogen bonding amongst the small subset of molecules. We have performed optimization and frequency calculation for all the snapshots for each system to obtain the spectrum. Finally, we averaged the spectra from all the different configurations to obtain the average spectrum for each system as shown in Fig. S11 in SI.

Now we can compare the origin of different modes from both classical normal mode analyses and quantum calculations. Both NMA and *ab initio* calculations suggest that the motions below 2 THz region involve movement of the whole alcohol molecules as shown in Fig. S8 in SI. This observation is consistent with all the alcohol systems studied here.

In the present study, we find that there is a strong absorption in the range of 4–6 THz. The peak position is also found to shift towards higher frequencies as we move from methanol to larger alcohols. Note that the modes in this region (Fig. 5) do not involve only hydrogen bond motion; rather the motion involves both OH groups and the alkyl chain.

To probe further into strength of H-bond in different alcohols, we calculated the variation of energy with respect to the H-bond distance as shown in Fig. 6. We see that methanol requires highest energy to break the H-bond and also it has higher frequency (from the curvature at the minimum) compared to other alcohols. Therefore, the peak due to H-bonded motion should appear at the highest frequency for methanol contrary to what is observed in the 4–6 THz range. This ascertains that the frequencies observed in the above region may appear due to the movement of alkyl chains rather than hydrogen bond (O··H) stretching. Interestingly, studies on ionic liquids show that a peak close to 6 THz (200 cm^{-1}) is present only when there is H-bonding present. Also, the frequency above 6 THz has been found to originate from H bonding in different other systems [32,33].

From the above observation and comparison with other systems we speculate that the H-bonded motions correspond to the experimental peaks above 8 THz. The modes at frequencies above 8 THz obtained from NMA are shown in Fig. S10 in SI. Thus, we can characterize the experimental peaks into the following types: the low frequency ones (below 2 THz) are likely to originate from the overall motion of the alcohol molecules, while the motion of the alkyl groups give rise to peaks in 4–6 THz range. Finally, the

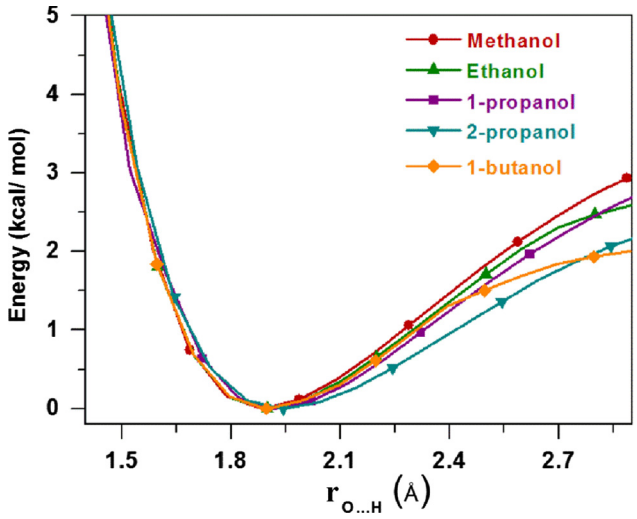

Fig. 6. The relative energy change as a function of H-bond distance for different systems. The energy values were calculated using constrained optimization using MP2/ aug-cc-pVDZ method.

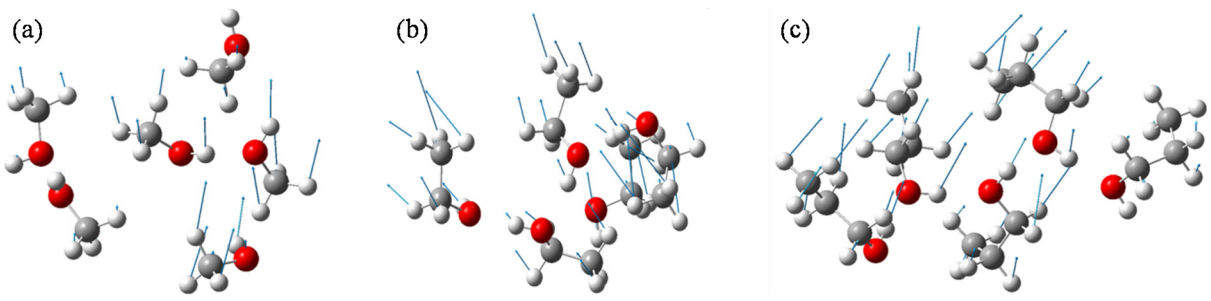

Fig. 5. The modes of the alcohol molecules around 4–6 THz region for methanol (a), ethanol (b), 1-propanol (c) using normal mode analyses. The arrows here indicate the movements of atoms in different directions. The larger arrows on H-atoms of the alkyl chains indicate larger movements of these compared to the hydroxyl hydrogen atoms.

peaks at higher frequencies involve H-bond movements. However, the reason behind the frequencies of all three oscillators to increase with the size of the alcohols is not understood, and further studies are required.

4. Conclusions

We have reported here experimental and theoretical investigations of dielectric response of five mono-hydroxy alcohols in broad THz frequency range (0.5–10 THz). Earlier experimental reports of similar systems were limited to 2.5 THz. Therefore, this study has widened the scope and understanding of the complex motions involved in these small molecules. We find that a model combining single Debye and triple damped harmonic oscillators satisfactorily reproduces the experimental complex dielectric spectra. With the help of MD simulations and quantum calculations we are able to evaluate the nature of dynamics that respond to our experimental spectral window (0.5–10 THz). However, while classical simulations are limited by the choice of the force-field, the quantum calculations suffer from the system size effect. Although the qualitative feature of the frequency dependence of the spectrum between 2–6 THz is similar between theory and experiment, a quantitative comparison was not possible for all alcohols. We have tried to identify the peaks observed in the dielectric loss spectra and ascribed them to a combination of vibrational modes involving motions of many atoms across several alcohol molecules in the networked structure. Primarily three types of motions were identified: the overall motion of alcohol molecules give rise to peak close to 2 THz, the peaks in intermediate frequency range (4–6 THz) are due to alkyl group oscillations, and the peaks at higher frequency range are probably the signatures of the movement of H-bonded OH groups of the alcohol molecules. Finally, we believe that the study carried out at a broad spectral range in THz frequency domain will enable researcher to choose these alcohols as a solvent prudently in THz experiments.

Acknowledgements

This work was supported by IISER Pune. PM (grant no. EMR/2016/003734) and AM (grant no. EMR/2016/001069) thank SERB, Department of Science and Technology, Government of India. SS thanks UGC, India for fellowship.

Appendix A. Supplementary material

Figures showing THz setup, time and frequency domain terahertz, contribution of Debye relaxation and three oscillators to the experimentally observed dielectric loss spectrum for methanol,VDOS from normal mode analysis, visual representations of vibrational modes, and average *ab initio* vibrational spectra; and tables containing errors in refractive index and dielectric constants for both real and imaginary parts, table containing fitting parameters with χ^2 and correlation coefficients. Supplementary data associated with this article can be found, in the online version, at http://dx.doi.org/10.1016/j.cplett.2017.04.026.

References

[1] (a) S.J. Grabowski in Hydrogen Bonding-New Insight, vol. 3, Springer, Dordrecht, The Netherlands, 2006.;
(b) G.C.M. Pimentel, A.L. McClellan, Annu. Rev. Phys. Chem. 22 (1971) 347–385.
[2] (a) M. Pagliai, G. Cardini, R. Righini, V. Schettino, J. Chem. Phys. 119 (2003) 6655–6662;
(b) V. Kumar Yadav, A. Chandra, Chem. Phys. 415 (2013) 1–7.
[3] (a) A.K. Karmakar, S. Sarkar, R.N. Joarder, J. Phys. Chem. 99 (1995) 16501–16503;
(b) S. Kashtanov, A. Augustson, J.-E. Rubensson, J. Nordgren, H. Ågren, J.-H. Guo, Y. Luo, Phys. Rev. B 71 (2005) 104205;
(c) S. Sarkar, R.N. Joarder, J. Chem. Phys. 99 (1993) 2032–2039;
(d) Y. Tanaka, N. Ohtomo, K. Arakawa, Bull. Chem. Soc. Jpn. 58 (1985) 270–276.
[4] R.Z. Ludwig, M.D. Zeidler, T.C. Farrar, Phys. Chem. 189 (1995) 19–27.
[5] K. Shinokita, A.V. Cunha, T.L.C. Jansen, M.S. Pshenichnikov, J. Chem. Phys. 142 (2015) 212450.
[6] K. Mazur, M. Bonn, J. Hunger, J. Phys. Chem. B 119 (2015) 1558–1566.
[7] (a) F.X. Hassion, R.H. Cole, J. Chem. Phys. 23 (1955) 1756–1761;
(b) C. Hansen, F. Stickel, T. Berger, R. Richert, E.W. Fischer, J. Chem. Phys. 107 (1997) 1086–1093;
(c) T. Sato, R. Buchner, J. Chem. Phys. 118 (2003) 4606–4613;
(d) T. Sato, R. Buchner, J. Phys. Chem. A 108 (2004) 5007–5015;
(e) U. Møller, D.G. Cooke, K. Tanaka, P.U. Jepsen, J. Opt. Soc. Am. B 26 (2009) A113–A125.
[8] (a) S.K. Garg, C.P. Smyth, J. Phys. Chem. 69 (1965) 1294–1301;
(b) J. Barthel, K. Bachhuber, R. Buchner, H. Hetzenauer, Chem. Phys. Lett 165 (1990) 369–373;
(c) R. Buchner, J. Barthel, J. Mol. Liq. 52 (1992) 131–144.
[9] (a) J.B. Baxter, G.W. Guglietta, Anal. Chem. 83 (2011) 4342–4368;
(b) C.A. Schmuttenmaer, Chem. Rev. 104 (2004) 1759–1780.
[10] J.T. Kindt, C.A. Schmuttenmaer, J. Phys. Chem. 100 (1996) 10373–10379.
[11] T. Fukasawa, T. Sato, J. Watanabe, Y. Hama, W. Kunz, R. Buchner, Phys. Rev. Lett. 95 (2005) 197802.
[12] (a) Y. Yomogida, Y. Sato, R. Nozaki, T. Mishina, J.I. Nakahara, J. Mol. Liq. 154 (2010) 31–35;
b) Y. Yomogida, Y. Sato, R. Nozaki, T. Mishina, J.I. Nakahara, J. Mol. Struct. 981 (2010) 173–178.
[13] (a) X. Xie, J. Dai, X.C. Zhang, Phys. Rev. Lett. 96 (2006) 075005;
(b) K.Y. Kim, A.J. Taylor, J.H. Glownia, G. Rodriguez, Nature Photon 2 (2008) 605–609;
(c) D.J. Cook, R.M. Hochstrasser, Opt. Lett. 25 (2000) 1210–1212.
[14] S. Nashima, O. Morikawa, K. Takata, M. Hangyo, J. Appl. Phys. 90 (2001) 837–842.
[15] W.L. Jorgensen, D.S. Maxwell, J. Tirado-Rives, J. Amer. Chem. Soc. 118 (1996) 11225–11236.
[16] T. Schlick, Molecular modeling and simulation: an interdisciplinary guide (2010).
[17] H.J.C. Berendsen, J.P.M. Postma, W.F. van Gunsteren, A. DiNola, J.R. Haak, J. Chem. Phys 81 (1984) 3684–3690.
[18] a) S. Nosé, Mol. Phys. 52 (1984) 255–268;
b) W.G. Hoover, Phys. Rev. A 31 (1985) 1695–1697.
[19] M. Parrinello, A. Rahman, J. Appl. Phys. 52 (1981) 7182–7190.
[20] T. Darden, D. York, L. Pedersen, J. Chem. Phys. 98 (1993) 10089–10092.
[21] D.E.Gray (Ed.), American Institute of Physics Handbook, McGraw-Hill Book Company, 1963.
[22] B. Hess, C. Kutzner, D. van der Spoel, E. Lindahl, J. Chem. Theory Comput. 4 (2008) 435–447.
[23] R. Dennington, T. Keith, J. Millam, Semichem Inc., Shawnee Mission KS, 2009.
[24] T. Yanai, D.P. Tew, N.C. Handy, Chem. Phys. Lett. 393 (2004) 51–57.
[25] M.A. Czarnecki, Y. Morisawa, Y. Futami, Y. Ozaki, Chem. Rev. 115 (2015) 9707–9744.
[26] a) P.D. Mitev, P.A. Bopp, J. Petreska, K. Coutinho, H. Ågren, L. Pejov, K. Hermansson, J. Chem. Phys. 138 (2013) 064503;
b) C.D. Daub, P.-O. Åstrand, F. Bresme, J. Phys. Chem. A 119 (2015) 4983–4992.
[27] T.H. Dunning, J. Chem. Phys. 90 (1989) 1007–1023.
[28] M.J. Frisch, G.W. Trucks, H.B. Schlegel, G.E. Scuseria, M.A. Robb, J.R. Cheeseman, G. Scalmani, V. Barone, B. Mennucci, G.A. Petersson, H. Nakatsuji, M. Caricato, X. Li, H.P. Hratchian, A.F. Izmaylov, J. Bloino, G. Zheng, J.L. Sonnenberg, M. Hada, M. Ehara, K. Toyota, R. Fukuda, J. Hasegawa, M. Ishida, T. Nakajima, Y. Honda, O. Kitao, H. Nakai, T. Vreven, J.A. Montgomery Jr., J.E. Peralta, F. Ogliaro, M.J. Bearpark, J. Heyd, E.N. Brothers, K.N. Kudin, V.N. Staroverov, R. Kobayashi, J. Normand, K. Raghavachari, A.P. Rendell, J.C. Burant, S.S. Iyengar, J. Tomasi, M. Cossi, N. Rega, N.J. Millam, M. Klene, J.E. Knox, J.B. Cross, V. Bakken, C. Adamo, J. Jaramillo, R. Gomperts, R.E. Stratmann, O. Yazyev, A.J. Austin, R. Cammi, C. Pomelli, J.W. Ochterski, R. L. Martin, K. Morokuma, V.G. Zakrzewski, G.A. Voth, P. Salvador, J.J. Dannenberg, S. Dapprich, A.D. Daniels, Ö. Farkas, J.B. Foresman, J.V. Ortiz, J. Cioslowski, D.J. Fox in Gaussian 09, vol. Gaussian Inc, Wallingford, CT, USA, 2009.
[29] a) J. McGregor, R. Li, J.A. Zeitler, C. D'Agostino, J.H.P. Collins, M.D. Mantle, H. Manyar, J.D. Holbrey, M. Falkowska, T.G.A. Youngs, C. Hardacre, E.H. Stitt, L.F. Gladden, Phys. Chem. Chem. Phys. 17 (2015) 30481–30491;
b) M. Koeberg, C.-C. Wu, D. Kim, M. Bonn, Chem. Phys. Lett. 439 (2007) 60–64;
c) K.J. Tielrooij, D. Paparo, L. Piatkowski, H.J. Bakker, M. Bonn, Biophys. J. 97 (2009) 2484–2492;
d) K.J. Tielrooij, N. Garcia-Araez, M. Bonn, H.J. Bakker, Science 328 (2010) 1006–1009.
[30] A.P. Sunda, A. Mondal, S. Balasubramanian, Phys. Chem. Chem. Phys. 17 (2015) 4625–4633.
[31] K.N. Woods, H. Wiedemann, J. Chem. Phys. 123 (2005) 134506.
[32] S.S. Sarangi, S.K. Reddy, S. Balasubramanian, J. Phys. Chem. B 115 (2011) 1874–1880.
[33] A. Mondal, S. Balasubramanian, J. Phys. Chem. B 119 (2015) 1994–2002.